Supporting Information

Strother et al. 10.1073/pnas.1703090115

SI Materials and Methods

Data Availability. All data, reagents, and code used in this manuscript will be provided upon request by M.B.R. (reiserm@janelia.hhmi.org).

Fly Stocks. Cell type-specific expression of the fluorescent calcium indicators (32) and Chrimson-tdTomato (46) was achieved using the GAL4/UAS, Split-GAL4/UAS, and LexA/LexAop (28–30). The selected drivers were described in previous studies (23, 38, 47), with the exception of R72E01-LexA, which targets expression to Mi4 and was selected by surveying a large collection of imaged driver lines, similar to those previously described (29, 31). Genotypes for each experimental animal are listed in Table S1. "*w+*(*DL*)" denotes an X chromosome from a particular wild-type laboratory strain derived by the laboratory of Michael Dickinson, California Institute of Technology, Pasadena, CA.

Immunohistochemistry and Imaging. All anatomical analyses were done using female flies. For the images in Figs. 1*B* and 3*A*, brains of female flies were dissected in PBS, fixed in PBS with 2% (vol/vol) paraformaldehyde (prepared from a 20% stock solution; #15713; Electron Microscopy Sciences) for 1 h at room temperature (RT) and washed three times with PBT [PBS with 0.5% (vol/vol) Triton X-100]. Samples were then incubated with PBT-NGS [5% (vol/vol) normal goat serum in PBT] for 30 min at RT, and then with primary antibodies [mouse anti-GFP mAb 3E6, #A-11120, Thermo Fisher Scientific, 1:100 dilution; rat anti-CadN mAb DN-Ex #8 (58), Developmental Studies Hybridoma Bank, 1:20 dilution; and rabbit anti-DsRed, #632496, Clontech, 1:1,000 dilution for Fig. 1*B*; and rabbit anti-GFP polyclonal, Thermo Fisher Scientific, #A-11122, 1:1,000 dilution; and mouse anti-Brp mAb Nc82 (59), Developmental Studies Hybridoma Bank, 1:50 dilution for Fig. 3*A*] in PBT-NGS at 4 °C overnight. This was followed by additional washes with PBT and incubation with secondary antibodies [DyLight 488-AffiniPure donkey anti-mouse IgG (H+L), Jackson ImmunoResearch Laboratories, #715-485-151, 1:500 dilution; DyLight 594 AffiniPure donkey anti-rabbit IgG (H+L), Jackson ImmunoResearch Laboratories, #711-515-152, 1:300 dilution; and Alexa Fluor 647 AffiniPure donkey anti-rat IgG (H+L), Jackson ImmunoResearch Laboratories, #712-605-153, 1:300 dilution for Fig. 1*B*; and Alexa Fluor 488 AffiniPure donkey anti-rabbit IgG (H+L), Jackson ImmunoResearch Laboratories, #711-545-152, 1:1,000 dilution; and Cy3 AffiniPure donkey anti-mouse IgG (H+L), Jackson ImmunoResearch Laboratories, #711-165-151, 1:300 dilution for Fig. 3*A*] in PBT-NGS at 4 °C overnight. After a final set of washes with PBT and then PBS, brains were mounted in Vectashield (Vector Laboratories) under a #1.5 coverslip and imaged on a Zeiss LSM 710 confocal microscope using a 40×, N.A. 1.3 (Fig. 1*B*), or a 20×, N.A. 0.8 (Fig. 3*A*) objective. For Multicolor FlpOut (MCFO) (57) labeling (Fig. 3*A*, *Left* side), brains were processed, mounted in DPX, and imaged with a 20×, N.A. 0.8 objective, as described (57). Brightness and contrast of individual channels were adjusted using Fiji (fiji.sc/).

Walking-Fly Behavioral Experiments. The methods used for these behavioral experiments have been detailed elsewhere (23) but are summarized here. For tethering flies, we first immobilize the wings of 2- to 4-d-old female flies with UV light-activated glue (KOA 300-1; KEMXERT) at least 12 h before the experiments. Each fly was tethered to a tungsten rod (catalog #71600; A-M Systems) using the same adhesive, and then placed in an incubator (model PH09-DM, Thermoelectric Series; Darwin Chambers Company) at 32 °C, 60% humidity, for ∼25 min before the behavioral tasks. During the experiments, tethered flies were positioned on a 9-mm-diameter, 129-mg styrofoam ball, which was supported by 340 SCCM airflow. The complete setup, which included the visual LED arena (40) and the treadmill system (39), was housed within the incubator. Behavioral experiments were conducted at 34 °C (measured near the air-supported ball), 60% humidity. We silenced the octopamine neurons by expressing Kir2.1 [using *pJFRC49-10XUAS-IVS-eGFP-Kir2.1(attP2)* (60)] in neurons labeled by the Tdc2-GAL4 driver (see Table S1 for complete genotype information). We confirmed the efficacy of this Kir2.1 effector by crossing to panneuronal GAL4 driver (R57C10) and confirming early larval lethality.

The ball movement is tracked by two optical flow cameras (ADNS-6090; Avago Technologies) that measure image displacements. The raw measurements were streamed at 4 kHz from the optic flow chips and summed into 20-ms bins, which are then acquired by a custom MATLAB program which runs the experiment. The camera data are transformed into 50-Hz measurements of forward/sideslip/turning (ball pitch/roll/yaw), in arbitrary units. These measurements of displacement are scaled by 50/s to generate velocity signals (arbitrary units per second).

The cylindrical visual arena was constructed from 36, 8 × 8-pixel LED modules, consisting of a 32 × 72 array of 525-nm peak emission LEDs (UltraPure Green LED; IO Rodeo), and spanning 270° in azimuth and 120° in elevation, the pixel size of each LED is at maximum ∼3.75°. The mean light power measured (using Thorlabs S170C power sensor) from the fly's vantage on top of the air-supported ball is ∼0.6 W/m^2 at 525-nm wavelength. We made use of an updated version of the display controller (IO Rodeo, www.iorodeo.com/; further details at https://bitbucket.org/mreiser/panels).

To test the visual responses of tethered walking flies, a series of behavioral experiments were performed (Fig. 3). A 30° spatial wavelength with ∼23% contrast ON/OFF grating pattern (bars illuminated at 5/15 and 8/15 of max intensity) was presented with five different stimulus movement durations (0.25, 0.5, 1, 2, and 4 s) and seven speeds (0.5, 2, 4, 8, 12, 16, and 24 Hz). After the moving visual stimulus, the final frame of each stimulus was presented statically for a period of 0.8 s. All trials were followed by a 1-s interstimulus interval, during which a homogeneous, full-field stimulus with intermediate intensity (5/15 max intensity) was presented. Within an experimental series, all visual stimuli were presented as symmetric pairs, consisting of clockwise (CW) and counterclockwise (CCW) versions of each stimulus condition (35 in each direction), with all 70 conditions presented using a random block trial structure (all trials repeated four times, within blocks consisting of all trial types in random order). The complete protocol consisted of 280 trials for each fly and lasted ∼20 min.

In the protocol, flies were presented with paired visual stimuli that moved either in the CW or CCW direction. For the data analysis, the mean yaw (turning) velocity of the behavioral response was calculated as follows:

$$\Delta\text{yaw} = \frac{\text{yaw}_{CW} - \text{yaw}_{CCW}}{2},$$

where Δyaw is the differential yaw velocity, and yaw_{CW} and yaw_{CCW} are the yaw velocities in response to a CW and CCW stimuli, respectively. All behavioral data were averaged on a per-fly basis to produce a mean (sign corrected) yaw (turning) and mean pitch (forward) velocity for each pair of symmetric visual

stimuli (CW/CCW rotation). In the absence of visual stimuli, we note that the experimental genotype expressing Kir2.1 in octopamine neurons significantly reduced walking speeds in comparison with the control genotypes (Fig. S2).

For data presented here, we plot the turning velocity averaged across flies as if all responses were for CW motion. When plotting behavioral turning and forward velocity time series (Fig. 3*C* and Fig. S2), we show the median ± SEM across flies (after data are averaged per fly, across trial replicates). The data are smoothed using a moving average across five neighboring (20-ms) data points. Most responses feature a large turning reaction and a decrease in forward locomotion that builds up over ∼500 ms. In response to our shortest interval moving stimuli, the behavioral reaction continues to increase in size after the stimulus movement terminates. To best capture these differences in responses between short and long interval stimuli, for statistical comparisons we used the mean response during the initial 1 s for all of the trials with 0.25- and 0.5-s trial length, and used the mean response during the entire stimulus period for all of the trials with longer trial length (1, 2, and 4 s). All data analysis was performed off-line using software written in MATLAB. In all behavioral results, n represents individual flies. Statistically significant differences are reported for the experimental genotype only for conditions found to be different from both control genotypes based on a two-tailed t test, followed by a correction for multiple comparisons. We used a false discovery rate controlling procedure (61) with $q = 0.05$. The forward walking data are also summarized as a probability distribution (Fig. S2*B*) generated as a histogram with 45 evenly spaced bins.

Calcium Imaging: In Vivo Preparation and Microscopy. All flies used for calcium imaging experiments were reared under standard conditions (60% humidity, 12-h light/12-h dark, 25 °C, cornmeal agar diet). All imaging experiments were performed on females 1–6 d posteclosion. Details of the preparation follow those of similar experiments (22). Briefly, flies were cold anesthetized and tethered to a fine wire at the thorax using UV-curing adhesive. The two most anterior legs (T1) were severed to prevent the animals from grooming their eyes and obstructing the visual field. A small drop of UV adhesive on the ventral surface of the thorax was used to encapsulate the severed T1 legs and immobilize the head at the proboscis. Tethered flies were subsequently positioned such that their head just protruded through a small cutout in a thin metal sheet that served as the bottom of the perfusion bath, and the head and thorax were secured to the sheet using UV adhesive. The back surface of the head was bathed in saline (103 mM NaCl, 3 mM KCl, 1.5 mM $CaCl_2$, 4 mM $MgCl_2$, 26 mM $NaHCO_3$, 1 mM NaH_2PO_4, 8 mM trehalose, 10 mM glucose, 5 mM TES, bubbled with 95% O_2/5% CO_2) (62), and the cuticle was dissected away to expose the brain. Muscles 1 and 16 (63) were severed to reduce motion of the brain within the head capsule, and the postocular air sac on the imaged side was removed to expose the medulla. The temperature within the bath itself was monitored using a small thermocouple probe placed near to the fly head (<2 mm; Physitemp IT-21), and all experiments were performed at 20 °C.

The medulla was imaged using a two-photon microscope (Prairie Ultima) with near-infrared excitation (930 nm; Coherent Chameleon Ultra II) and a 60× objective (Nikon CFI APO 60XW). The excitation power was never greater than 25 mW at the sample. Imaging parameters varied slightly between experiments but were typically acquired at 128 × 128-pixel resolution, ∼10-Hz frame rate, and with a 100-μm field of view.

During imaging, the fly would show periods of motionlessness and rapid leg movements. A camera and right angle mirror were positioned under the fly to record the body of the fly and this behavior (Basler A622F; 30 Hz; 640 × 480 pixels; Computar MLM3X-MP). Camera recordings were synchronized with the two-photon microscope by configuring PrairieView to pulse a near-infrared LED positioned below the animal every 60 s of imaging. Those pulses were readily detected in the recorded camera images and used to synchronize the calcium imaging and behavioral imaging time series.

Calcium Imaging: Visual Stimuli. All visual stimuli were produced using a custom rear-projection system (22). The projection screen was positioned to provide a unilateral stimulus to the right eye and was centered around a point ∼45° from the sagittal plane and 10° above the equator of the eye. The corresponding region of the medulla was identified by displaying a small flickering disk near the center of the screen and surveying the medulla for a localized calcium response. Local retinotopy was verified before recording by confirming that small changes in stimulus position resulted in small shifts in the location of the most active medulla column.

Stimuli were grouped into sets that included appropriate control stimuli and could be presented in short protocols so that only negligible photobleaching occurred over the duration of the set. Results from four stimulus sets are presented: spontaneous (Fig. 2 *A* and *B*), air puffs (Fig. 2 *C* and *D*), moving gratings (Fig. 4 *B*–*D*), and moving gratings with CDM (Fig. 4 *E* and *F*). The "spontaneous" stimulus consisted of a 5-min interval during which the animal was in a completely dark environment, and the spontaneous responses of the animal were recorded. The "air puff" stimulus consisted of six to seven air puffs manually delivered through a tube positioned beneath the animal at 30-s intervals, while the animal was in a completely dark environment. The "moving gratings" stimulus set consisted of a square wave grating of dark (0% maximum intensity) and bright (100% maximum intensity) bars with a 30° period that spanned an area of ∼120° in the dorsoventral direction and ∼90° in the anterior–posterior direction. The grating moved in either the anterior-to-posterior direction or posterior-to-anterior direction at speeds of 30°/s, 90°/s, 180°/s, 270°/s, 810°/s, or 2,430°/s (set includes all combinations of direction and speed). Square wave gratings were presented for an 8-s interval with a 5-s interstimulus interval (full-field gray background), and six replicates were collected for each stimulus. The "moving gratings with CDM" stimulus set was identical to the "moving gratings" stimulus with the exception that bath water was replaced with saline containing 10 μM chlordimeform (CDM). The animal was allowed to incubate in the CDM saline for ∼5–10 min before imaging.

Calcium Imaging: Data Analysis. Data were analyzed using custom-written software (MATLAB; Mathworks). For all experiments, images were preprocessed to reduce lateral motion by shifting the images to maximize the correlation with a reference image (23) (https://bitbucket.org/jastrother/neuron_image_analysis).

An instantaneous, dimensionless movement index was calculated based on the images of the body of the fly recorded from below the animal. A region of interest (ROI) was selected adjacent to the body of the animal that included the legs of the animal. The leg movements of the animal were quantified by calculating the absolute value of the time derivative of the light intensity for the pixels within this ROI. This measure was smoothed using a boxcar filter (1 s); the measure was then shifted and scaled such that the 2.5% quantile had a value of zero and the 97.5% quantile had a value of 1, and the absolute value of the measure was taken to eliminate negative values. The resulting quantity was treated as an instantaneous, dimensionless measure of fly movement.

The spontaneous responses of the animal to a dark environment (Fig. 2 *A* and *B*) were analyzed by calculating the mean fluorescence for a ROI that included the top 95% brightest pixels in the imaged neuropil. The baseline fluorescence was calculated as the 10% quantile over the entire stimulus. The $\Delta F/F$ was calculated by subtracting the baseline fluorescence from the instantaneous fluorescence, and then normalizing the result by the baseline fluorescence. An example of the instantaneous $\Delta F/F$ is shown in

Fig. 2. To examine the relationship between the movement of the animal and the $\Delta F/F$, we computed the convolution kernel that best predicts the $\Delta F/F$ using the dimensionless movement index as input. For each fly, this convolution kernel was computed for an interval of time as follows:

$$g(\tau) = \mathcal{F}^{-1}\left[\frac{\mathcal{F}[M]^{*}\mathcal{F}[\Delta F/F]}{\mathcal{F}[M]^{*}\mathcal{F}[M] + N^{2}}\right],$$

where $\mathcal{F}$ and $\mathcal{F}^{-1}$ are the Fourier transform and its inverse, M is the dimensionless movement index, $\Delta F/F$ is the instantaneous normalized fluorescence, $g(\tau)$ is the computed convolution kernel, and N is a noise factor. The noise factor N limits the magnitude of the Fourier transform of the convolution kernel at higher frequencies where the movement index has little signal power and the resulting SNR is very low, and was selected empirically as the lowest value that suppressed high-frequency noise in the convolution kernel (N = 7.5e-3 for fast Fourier transform normalized by sample count, which corresponds to an $N^2 \sim 10\%$ of the mean power). A local convolution kernel was computed for a moving window (15-s period) that was passed over the entire time series, and a global convolution kernel was calculated as the average of the local convolution kernels. The global convolution kernel was then scaled by a constant factor such that the predicted $\Delta F/F$ (the convolution of the global convolution kernel and the movement index) best fit the measured $\Delta F/F$ in the least-squares sense. The convolution kernel computed for each individual fly had a similar shape, but the magnitude of the convolution kernel was variable. To minimize the effects of this variation in subsequent analyses, the convolution kernel for each individual fly was normalized by the SD of the $\Delta F/F$ recorded for the entire trial for that individual. To identify whether the convolution kernel was statistically distinguishable from zero, the average of the normalized convolution kernel for the period from −1 to 1 s was calculated for each individual, and this was compared with zero using a two-tailed t test. The computed convolution kernels are presented in Fig. 2 as the median across individuals with 25% and 75% quantiles. Although the median kernel was computed from the normalized kernels, to improve interpretability this kernel was scaled by the median normalization factor across individuals so that it could be presented on an unnormalized scale.

The responses of the animal to the air puff stimulus (Fig. 2 *C* and *D*) were examined by calculating the mean fluorescence for a ROI selected as above. The baseline fluorescence was calculated as the 10% quantile over the entire stimulus set. The $\Delta F/F$ was calculated by subtracting the mean fluorescence for the 1-s period before the air puff from the instantaneous fluorescence, and then normalizing the result by the baseline fluorescence. Although most individual flies responded similarly to air puffs, the magnitude of the calcium response recorded for individual flies was again variable. To reduce the impact of this variation, the computed $\Delta F/F$ values for each fly were normalized by the maximum $|\Delta F/F|$ observed in response to the first air puff. The normalized responses to the subsequent air puffs were then stimulus-aligned and averaged. To determine whether the animals showed a significant response to air puffs, the mean of the stimulus-aligned $\Delta F/F$ during the 1 s following the air puff was calculated for each individual, and this was compared with zero using a one-sample two-tailed t test. The responses to air puffs are presented similarly to the spontaneous-response convolution kernels, as the median across individuals scaled by the median normalization factor with 25% and 75% quantiles.

Responses to the moving-grating stimulus (Fig. 4) were analyzed by calculating the mean fluorescence for a manually selected ROI that encompassed the axon terminals of five to eight columns with receptive fields at the center of the display. The baseline fluorescence was calculated as the 10% quantile over the entire stimulus set. The $\Delta F/F$ was calculated by subtracting the mean fluorescence for the 2-s period before the start of each grating stimulus from the instantaneous fluorescence, and then normalizing the result by the baseline fluorescence.

To examine the effects of spontaneous movement, the trials from the moving-grating stimulus set were separated based on the average movement during the 2-s period before the start of each grating stimulus. Trials during which the nondimensional movement value was greater than a fixed threshold (0.2) were treated as "moving," while other trials were treated as "not-moving." Since the movement of the animal was spontaneous and largely unsynchronized with the stimulus presented, the number of moving and nonmoving trials produced by each individual animal for each stimulus was highly variable. Consequently, data from all individuals were pooled. The mean $\Delta F/F$ for the period 1–3 s after the start of the stimulus was compared between the moving and nonmoving trials using a one-tailed t test (Fig. 4*C*). Results were corrected for multiple comparisons by controlling the false discovery rate using the Benjamini–Hochberg procedure (q = 0.05), which was applied separately to each input neuron type for the set of tests that includes all combinations of grating direction and frequency.

The effects of CDM were examined by comparing the responses observed during the moving gratings and moving gratings with CDM stimulus sets. The $\Delta F/F$ values were computed as described above for moving bar trials without CDM. The responses recorded with CDM in the saline were not sorted into moving and not-moving conditions. Instead, the collective CDM dataset was compared against the CDM-free nonmoving responses, using a two-tailed t test (Fig. 4*E*). Results were corrected for multiple comparisons by controlling the false discovery rate using the Benjamini–Hochberg procedure (q = 0.05), which was applied separately to each input neuron type for the set of tests that includes all combinations of grating direction and frequency. In addition, the baseline shift produced by application was calculated (Fig. S1*E*) as the baseline fluorescence with CDM minus the baseline fluorescence without CDM, normalized by the average of the baseline fluorescence with and without CDM. For these calculations, the baseline fluorescence was taken as the mean fluorescence for the 2-s period before the start of the moving grating stimulus, averaged across all stimulus presentations. Significant differences between the CDM and control conditions were detected using an unpaired, two-tailed t test.

Functional Connectivity Experiments. Flies were reared at 25 °C on retinal supplemented (0.2 mM) cornmeal medium in vials that were shielded from light by foil wrapping. All experiments were performed on female flies, 1–2 d after eclosion. Brains with intact laminas were excised from flies in a Sylgard-lined dish filled with saline (103 mM NaCl, 3 mM KCl, 2 mM $CaCl_2$, 4 mM $MgCl_2$, 26 mM $NaHCO_3$, 1 mM NaH_2PO_4, 8 mM trehalose, 10 mM glucose, 5 mM TES, bubbled with 95% O_2/5% CO_2). After dissection, each brain was positioned posterior side up on an uncoated coverslip in the same dish and perfused with 20 °C saline.

The sample was imaged with a resonant scanning two-photon microscope with near-infrared excitation (920 nm, 5–11 mW at sample, Spectra-Physics, InSight DS Dual) and a 25× objective (Nikon MRD77225 25XW). The microscope was controlled by using ScanImage 2015.v3 (Vidrio Technologies). Images were acquired with a ∼235 × ∼235-μm field of view, with a resolution of 512 × 512 pixels, and an acquisition frame rate of ∼44 Hz. The presented time series data are based on down-sampled data, where five consecutive frames are averaged together for an ∼9-Hz frame rate.

For the photoactivation experiments, the light-gated ion channel Chrimson was activated with a 660-nm peak emission LED (M660L3; Thorlabs) coupled to a digital micromirror device (DLPC300 Light Crafter; Texas Instruments) and combined with

the imaging path via a FF757-DiO1 dichroic (Semrock), to project through the microscope objective. On the emission side, the primary dichroic was Di02-R635 (Semrock), the detection arm dichroic was 565DCXR (Chroma), and the emission filters were placed before the detectors to prevent saturation during photoactivation periods: FF03-525/50 (Semrock; for the green channel) and FF01-625/90 (Semrock; for the red channel). For nearly all experiments, photoactivation light was delivered in a pulse train that consisted of five 1-s pulses (100% duty cycle during each 1-s pulse), with a 60-s interval of no stimulation between the pulses. The light intensity was increased for each of the five pulses (0.1, 0.2, 0.4, 0.6, and 0.8 mW/mm^2; measured using Thorlabs S170C). For the experiments where Mi4 expressed GCamp6f (Fig. S4*C*), 0.8 mW/mm^2 photoactivation light was delivered in a pulse train that consisted of five 0.25-s pulses, with a 10-s interval of no stimulation in-between the pulses. The data in Fig. S4*C* are averaged, per brain, across these five pulses.

Two-color images (Figs. 5*C* and 6 *C* and *D*, and Figs. S3*A* and S4*A*) were collected with the same two-photon microscope used for the functional connectivity photoactivation experiments. The excitation wavelength was changed to 1,025 nm, which can effectively excite both GCaMP6 and Chrimson-tdTomato. The emission signals were collected simultaneously through the green and red channels. Brightness and contrast of the individual channels were adjusted using Fiji (fiji.sc/).

The calcium responses of the genetically targeted neurons were used to quantify the $\Delta F/F$ for a manually defined ROI. The $\Delta F/F$ was taken as $(F - F_o)/F_o$, where F is the instantaneous fluorescence averaged over the ROI and F_o is the fluorescence averaged over the ROI for a 5-s interval GCaMP6s experiments (and 2-s interval for GCaMP6f experiments), before the start of the photoactivation protocol. Responses to different photoactivation intensities and to variable CDM concentrations were compared by calculating the median $\Delta F/F$ for a fixed time period following the start of photoactivation (1–5 s after the start for the experiments with GCaMP6f; 1–10 s after the start of the experiments with GCaMP6s). All data analysis was performed off-line using software written in MATLAB.

The effect of octopamine modulation on the functional connectivity between L5 and Mi4 neurons was examined by adding the octopamine agonist CDM (chlordimeform hydrochloride; Sigma-Aldrich) to the saline bath. For +CDM trials, brains were dissected in saline with CDM and kept in the same bath during the photoactivation and imaging experiments. Brains were incubated in the +CDM bath for at least 5 min before imaging, and all imaging was completed within 20 min following dissection. For the control groups, CDM-free saline was used for both the dissection and imaging. Statistically significant differences between the calcium responses of the CDM-treated brains and the control brains were identified using a t test followed by false discovery rate correction (five P values for the five pulses experiment, $q = 0.05$).

Computational Modeling. To examine how different filtering strategies might affect the frequency tuning of a motion detector, we constructed a simple computational model of a Hassenstein–Reichardt correlator (HRC). We examined two variants of this model, one in which modulated filters were placed before the nonlinear element (i.e., correlator) and a second in which a modulated filter was placed after the nonlinear element (Fig. 7). These models were implemented as ordinary differential equations that were solved using a Runge–Kutta solver (MATLAB R2016a, ode45). The photoreceptors were assumed to respond linearly to the luminance at two adjacent points in the visual space (5° separation), the modulated filters were implemented as first-order low-pass filters with a variable time constant (τ_M = 5–200 ms), the HRC time delay was also implemented as first-order low-pass filter (τ_{HR} = 50 ms), the correlator was treated as a four-quadrant multiplier, and the input stimulus was a sinusoidal grating (30° period, zero offset). The model was solved for a fixed time period (~10 s rounded to a multiple of the grating period), and the presented responses are the mean of the output for the duration of the simulation.

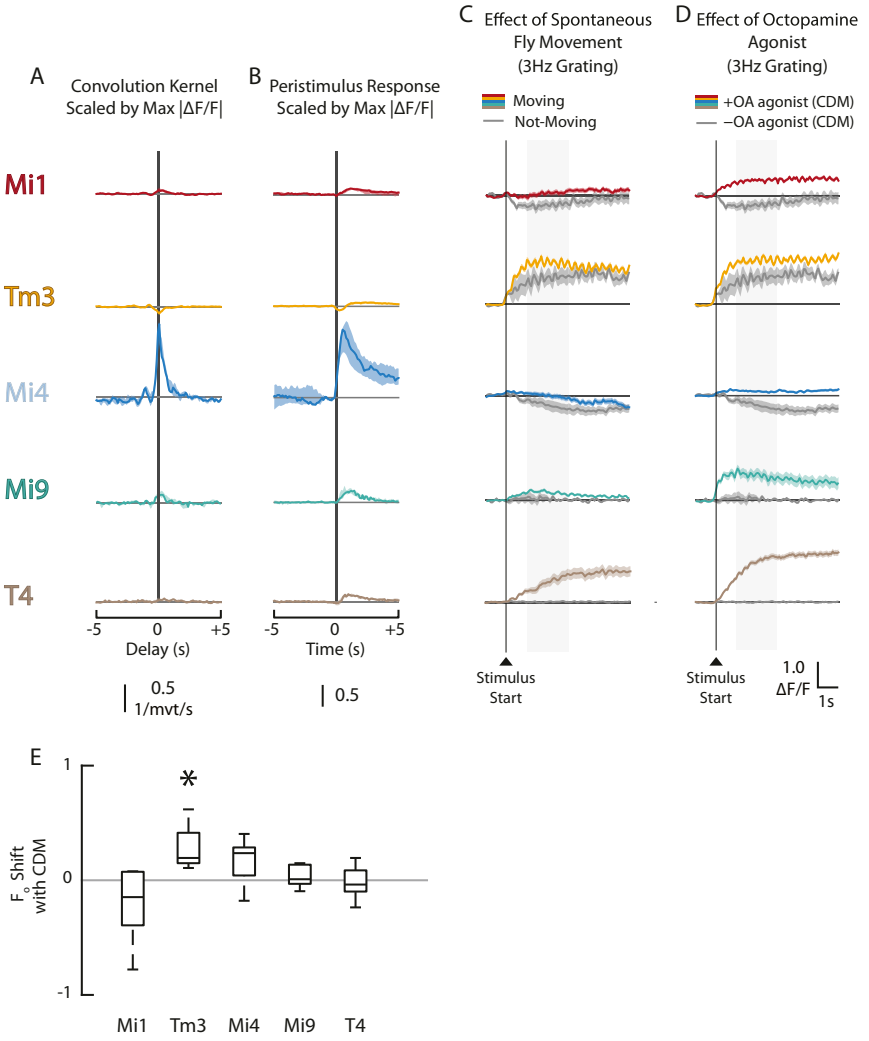

Fig. S1. Behavioral state affects the responses of T4 input neurons. (*A* and *B*) Additional analysis of the results presented in Fig. 2. Since the magnitude of the Δ*F*/*F* response can vary between neuron types, the convolution kernel and peristimulus responses of Fig. 2 are replotted here normalized by the maximum absolute Δ*F*/*F* value observed for each neuron type in response to moving gratings (peak of black lines in Fig. 4C). Since Mi4 responses to visual stimuli have modest Δ*F*/*F* values, this normalization procedure increases the relative size of the Mi4 responses and provides further evidence that Mi4 is unusually sensitive to the behavioral state of the animal. (*C* and *D*) Additional results from the experiments shown in Fig. 4. Time series of axonal calcium responses (Δ*F*/*F*) of Mi1, Tm3, Mi4, Mi9, and T4 neurons to a grating moving at 90°/s (corresponding to 3-Hz temporal frequency, 30° period, 100% contrast, anterior to posterior). The start of the stimulus is indicated by a vertical line. The responses are from multiple individuals ($n = 5$ for each genotype, same individuals as in Fig. 4) and are presented here as median values (±SEM). Although the neurons would be expected to show oscillations in activity at the grating frequency, such oscillations are attenuated by the slow kinetics of the calcium indicator. Instead of measuring these attenuated oscillations, tuning curves (Fig. 4) were constructed from the time-averaged Δ*F*/*F* during the stimulus presentation (averaged intervals indicated here by shaded areas). The responses to other gratings frequencies were similar in appearance, except that they approached different asymptotic values and the oscillations in Δ*F*/*F* were less attenuated at the slowest grating speed (1 Hz). (*E*) Shift in baseline fluorescence for experiments presented in Fig. 4*E*. The shift in baseline fluorescence was calculated as the baseline fluorescence with CDM minus the baseline fluorescence without CDM, normalized by the average of the baseline fluorescence with and without CDM. The responses are from multiple individuals ($n = 5$ for each genotype) and are presented as boxplots, where the central mark represents the median, the top and bottom edges represent the 25th and 75th percentiles, respectively, and whiskers represent the most extreme data points that were not outliers. Asterisks indicate baseline shifts that are significantly different from zero, as tested using an unpaired, two-tailed *t* test ($P > 0.05$).

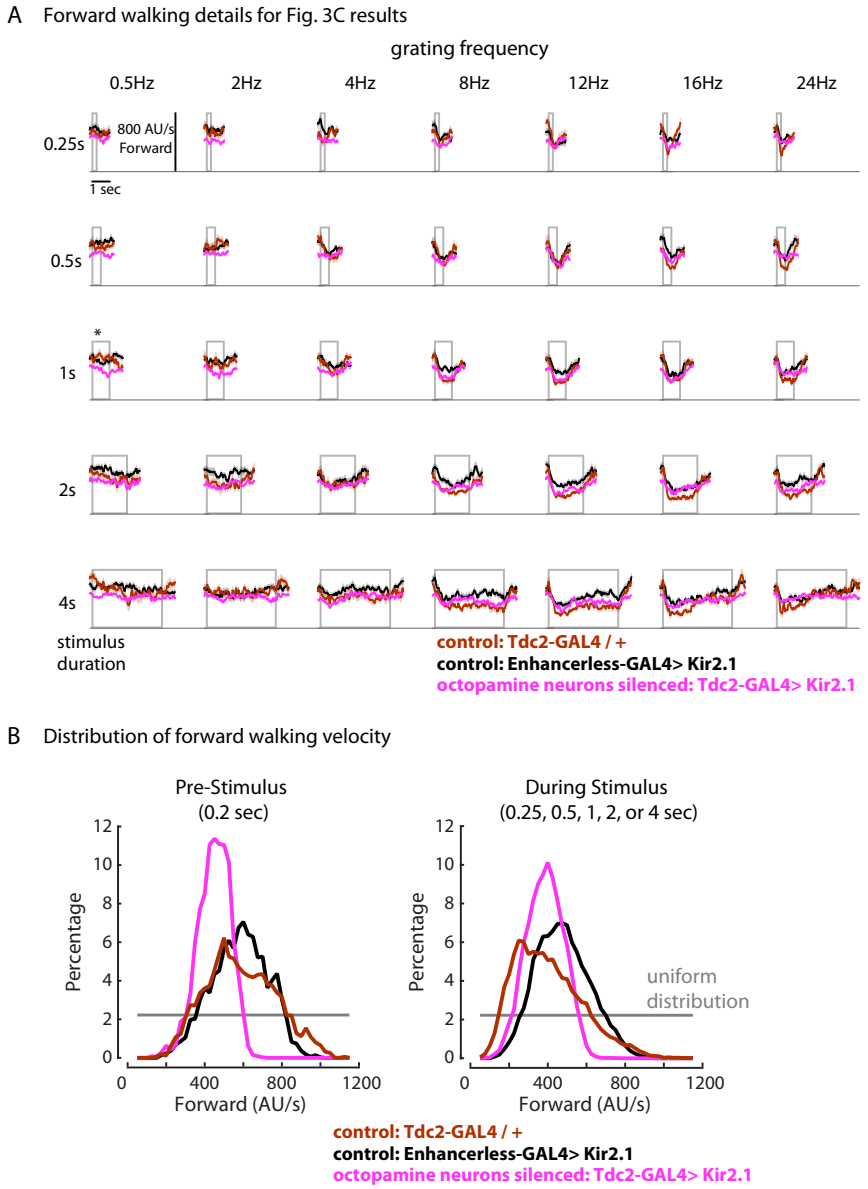

Fig. S2. Effects of silencing octopamine neurons on forward locomotion during visual motion stimulation. (*A*) The forward walking speed of flies (represented as arbitrary units; *Materials and Methods*) during the presentation (Fig. 3*C*) of rotational grating motion at different speeds (0.5–24 Hz) and different stimulus durations (0.25–4 s). The magenta lines represent the behavioral responses of flies with silenced octopamine neurons, while the black and brown lines represent the responses of control genotypes (Table S1 for details). The gray box represents the period of stimulus movement. Results shown are the median values (±SEM) from multiple flies ($n = 10$ individuals for all genotypes). Flies slow down while turning, and this decrease in forward movement is most prominent at higher stimulus speeds and during longer-duration stimuli. However, silencing octopamine neurons does not significantly alter this reduction in forward locomotion. The mean response differs significantly from both control lines (*t* test controlled for false discovery rate, $P < 0.05$) in only a single condition, indicated by an asterisk. (*B*) The distribution of forward walking velocity of all genotypes during the 0.2 s before (*Left*) and during (*Right*) the presentation of rotational visual motion. The forward walking velocities are displayed as a histogram (computed from 45 bins of the forward walking velocities in arbitrary units). As a reference, the uniform distribution is shown as a gray line. Silencing octopamine neurons reduces the speed of forward locomotion in the intervals preceding visual stimulation (based on means of all flies for comparison between experimental and both control genotypes; $P < 0.05$, *t* test), but not strongly during visual motion epochs (*t* test: $P < 0.05$ for comparison with Enhancerless-GAL4 > Kir2.1, but $P = 0.12$ for comparison with Tdc2-GAL4/+). Rather, the primary effect is seen to be a reduction in the modulation of walking speeds, as the histogram for the octopamine silenced genotype is narrower than for the two control genotypes ($P < 0.05$, *F* test of equality of variances, for all four comparisons to prestimulus and during-stimulus control genotype data).

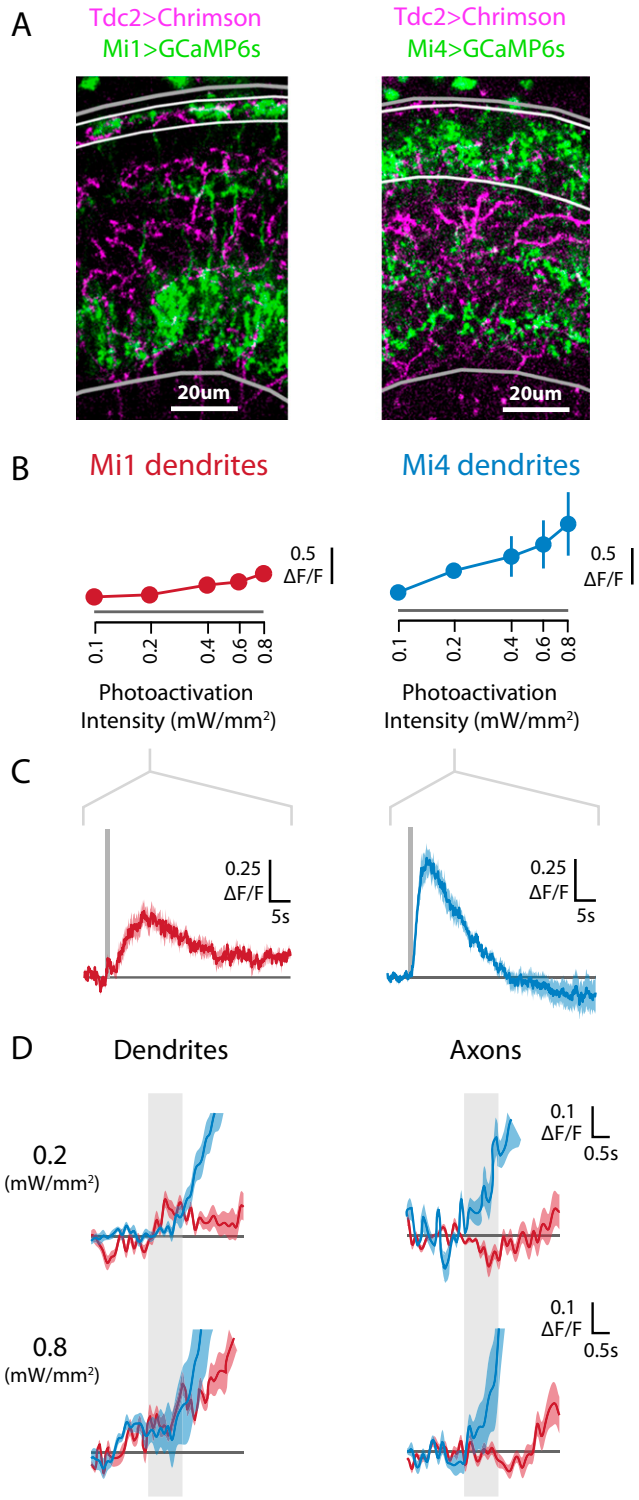

Fig. S3. Detailed calcium responses of Mi1 and Mi4 to photoactivation of the octopamine neurons. Further data analysis from the experiments presented in Fig. 5 (details follow those of the Fig. 5 legend). (*A–C*) Dendritic calcium responses of Mi1 and Mi4 to photoactivation of the octopamine neurons ($n = 6$ for both subsets). Region of interest (ROI) is outlined with white lines, and medulla is outlined with gray lines. (*D*) Time series of the initial calcium responses to photoactivation of octopamine neurons. The red and cyan lines represent the responses of Mi1 ($n = 6$) and Mi4 ($n = 6$), respectively. Results are shown as the median ± SEM $\Delta F/F$ for photoactivation intensities of 0.2 mW/mm^2 (*Top*) and 0.8 mW/mm^2 (*Bottom*). Responses are presented for both the dendrites (*Left*) and axons (*Right*). The stimulation period (1 s) is shown as gray vertical bars.

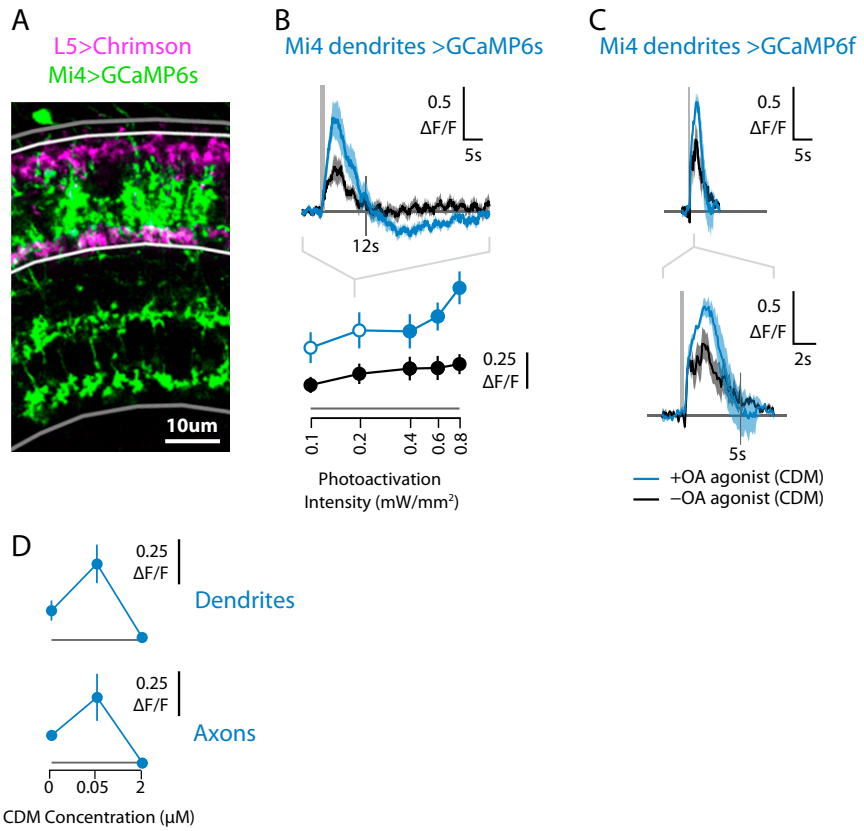

Fig. S4. CDM modulates axonal and dendritic compartments of Mi4. (*A* and *B*) Mi4 dendritic calcium responses from the main experiments in Fig. 6. See legend of Fig. 6 for detailed information. Region of interest (ROI) for analysis of the calcium response is outlined with white lines, and medulla is outlined with gray lines. (*C*) Time series of Mi4 dendritic calcium response (with Mi4 neurons expressing GCaMP6f) to brief (250-ms) pulses of L5 photoactivation (at 0.8 mW/mm^2, 660 nm). The blue line represents the response with the addition of the octopamine agonist CDM (50 nM) to the saline, and the black line shows response in the absence of CDM. The photoactivation period is indicated with a gray vertical bar. Data are presented as median ± SEM Δ*F*/*F* from multiple brains ($n = 3$ for each +CDM and –CDM). The *Top* is shown on the same timescale as the GCaMP6s responses in *B*, while the *Bottom* is plotted on an expanded timescale to show the finer structure of these responses. To compare the kinetics of these responses, the approximate time points where these responses have returned to prestimulation levels are indicated. (*D*) Tuning curves of the Mi4 calcium responses (expressing GCaMP6s) to L5 photoactivation (mean during the first 10 s after start of photoactivation) with different CDM concentrations [CDM free ($n = 6$), 0.05 μM ($n = 6$), and 2 μM ($n = 4$); brains were stimulated at 0.1 mW/mm^2, 660 nm]. Results are presented as the mean ± SEM Δ*F*/*F* value for the dendritic branches (*Top*) and axonal terminals (*Bottom*; strata M10).

Table S1. The complete list of fly genotypes used in the experiments presented throughout this manuscript

Stock genotype	Cells manipulated/ effector	Cells imaged/indicator	Used in figure
LexAop2-Syn21-opGCaMP6s(su(Hw)attP8),10XUAS-Syn21-Chrimson88-tdT-3.1(attP18)/w^{1118}; R42F06-LexA(su(Hw)attP5), R42F06-LexA(VK00022)/+; Tdc2-GAL4(attP2)/+	None	T4,T5/opGCaMP6s (anti-GFP) Tdc2/Chrimson88 (anti-dsRed)	Fig. 1
w+(DL)/w^{1118}; +/R55C05-p65ADZp(attP40); pGP-JFRC7-20XUAS-IVS-GCaMP6f(VK00005)/R71D01-ZpGdbd(attP2)	None	Mi1/GCaMP6f	Fig. 2 Fig. 4 Fig. S1
w+(DL)/w^{1118}; +/R38C11-p65ADZp(attP40); pGP-JFRC7-20XUAS-IVS-GCaMP6f(VK00005)/R59C10-ZpGdbd(attP2)	None	Tm3/GCaMP6f	Fig. 2 Fig. 4 Fig. S1
w+(DL)/w^{1118}; +/R48A07-p65ADZp(attP40); pGP-JFRC7-20XUAS-IVS-GCaMP6f(VK00005)/R79H02-ZpGdbd(attP2)	None	Mi4/GCaMP6f	Fig. 2 Fig. 4 Fig. S1 Movie S1
w+(DL)/w^{1118}; +/R48A07-p65ADZp(attP40); pGP-JFRC7-20XUAS-IVS-GCaMP6f(VK00005)/VT046779-ZpGdbd(attP2)	None	Mi9/GCaMP6f	Fig. 2 Fig. 4 Fig. S1
w+(DL)/w^{1118}; R42F06-LexAp65(su(Hw)attP5)/+; pJFRC99-20XUAS-IVS-Syn21-Shibire-ts1- p10(VK00005), pGP-JFRC59-13XLexAop2-IVS-p10-GCaMP6m(su(Hw)attP1)/pDPGal4U(attP2)	None	T4,T5/GCaMP6m	Fig. 2 Fig. 4 Fig. S1
w+(DL)/w^{1118};+(DL)/+;pJFRC49-10XUAS-IVS-eGFP-Kir2.1(attP2)/Tdc2-Gal4(attP2)	Tdc2/Kir2.1	Tdc2 (anti-GFP)	Fig. 3 Fig. S2
R57C10-Flp2::PEST (attP18);;JFRC201-10XUAS-FRT > STOP > FRT-myr::smGFP-HA (VK0005), pJFRC240-10XUAS-FRT > STOP > FRT-myr::smGFP-V5-THS-10XUAS-FRT > STOP > FRT-myr::smGFP-FLAG (su(Hw)attP1)/Tdc2-GAL4(attP2)	None	Tdc2/MCFO-7	Fig. 3
Control stock: *w+(DL)/w^{1118};+(DL)/+;pJFRC49-10XUAS-IVS-eGFP-Kir2.1(attP2)/pDPGal4U(attP2)*	None/Kir2.1	None	Fig. 3 Fig. S2
Control stock: *w+(DL)/w^{1118};+(DL)/+;+(DL)/Tdc2-Gal4(attP2)*	Tdc2/none	None	Fig. 3 Fig. S2
LexAop2-Syn21-opGCaMP6s(su(Hw)attP8),10XUAS-Syn21-Chrimson88-tdT-3.1(attP18)/w^{1118}; R19F01-LexA(su(Hw)attP5)/+; Tdc2-GAL4(attP2)/+	Tdc2/Chrimson88	Mi1/opGCaMP6s	Fig. 5 Fig. S3
LexAop2-Syn21-opGCaMP6s(su(Hw)attP8),10XUAS-Syn21-Chrimson88-tdT-3.1(attP18)/w^{1118}; R72E01-LexA(attP40)/+; Tdc2-GAL4(attP2)/+	Tdc2/Chrimson88	Mi4/opGCaMP6s	Fig. 5 Fig. S3
20XUAS-IVS-Syn21-opGCaMP6f-p10(su(Hw)attP8)/10XUAS-Syn21-Chrimson88-tdT-3.1(attP18); R64B07-p65ADZp(attP40)/+; R37E10-ZpGdbd(attP2)/+	L5/Chrimson88	L5/opGCaMP6f	Fig. 6
LexAop2-Syn21-opGCaMP6s(su(Hw)attP8),10XUAS-Syn21-Chrimson88-tdT-3.1(attP18)/w^{1118}; R72E01-LexA(attP40)/R64B07-p65ADZp(attP40); R37E10-ZpGdbd(attP2)/+	L5/Chrimson88	Mi4/opGCaMP6s	Fig. 6 Fig. S4
LexAop2-Syn21-opGCaMP6f(su(Hw)attP8),10XUAS-Syn21-Chrimson88-tdT-3.1(attP18)/w^{1118}; R72E01-LexA(attP40)/R64B07-p65ADZp(attP40); R37E10-ZpGdbd(attP2)/+	L5/Chrimson88	Mi4/opGCaMP6f	Fig. S4

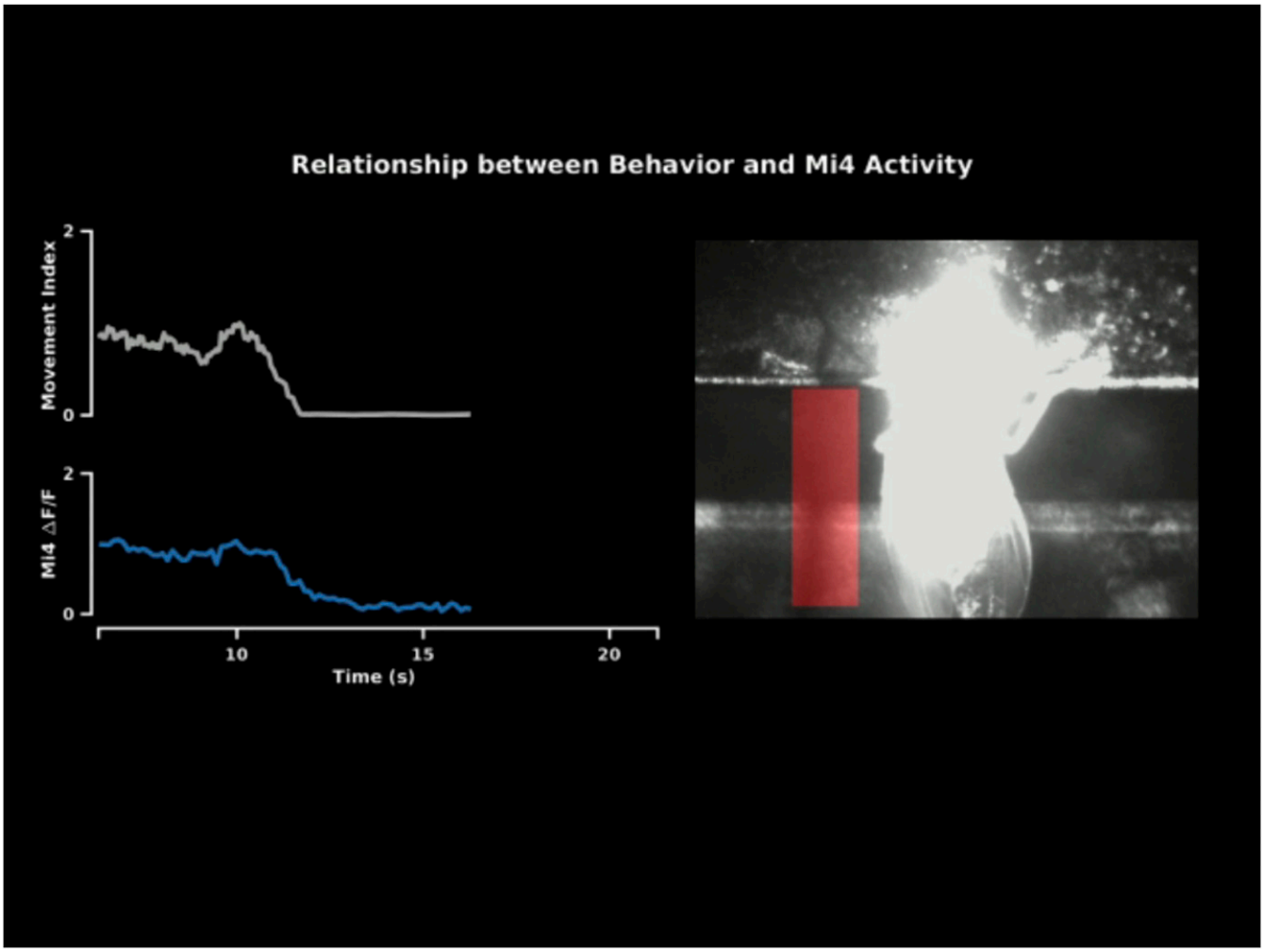

Movie S1. Relationship between behavior and Mi4 activity. Movie demonstrating leg movements of tethered fly with a synchronized time series showing the calculated movement index and the simultaneously recorded $\Delta F/F$ for Mi4 neurons. The responses were recorded in a dark environment without visual stimuli; they are shown here at 1× speed; the fly behavior is shown from a ventral perspective, and a red shaded rectangle indicates the ROI used for the calculation of the movement index. Although the near-infrared two-photon laser light is outside of the visual range of the flies, it is within the spectral range of the camera and saturates some pixels over the body of the fly. In the beginning of the movie, the fly demonstrates spontaneous leg movements which correlate with increases in the $\Delta F/F$ of Mi4 neurons. Starting at ~38 s into the movie, three air puffs are delivered at 30-s intervals which produce sharp increases in behavioral activity and Mi4 calcium activity. After the time series plays through at 1× speed, the movie shows the time periods around the air puffs slowed down to 1/3× speed. The tethering of the flies prevents prevent prolonged flight bouts, but air puffs produced a brief period of wing flutter. This wing flutter is subtle but can observed as a rapid and marked blurring of the wings. During these periods, the words "wing flutter" appear in red letters over the video of the fly. Finally, since the calculation of the movement index includes a boxcar low-pass filter, the movement index does not respond instantly to changes in the fly's movement. Also, because calcium data were recorded independently of behavioral data and then synchronized post hoc, these data are only synchronized to within one frame period.

Movie S1